Understanding the Changes of Stratospheric Water Vapor in Coupled Chemistry–Climate Model Simulations

LUKE OMAN AND DARRYN W. WAUGH

Department of Earth and Planetary Sciences, The Johns Hopkins University, Baltimore, Maryland

STEVEN PAWSON

Global Modeling and Assimilation Office, NASA Goddard Space Flight Center, Greenbelt, Maryland

RICHARD S. STOLARSKI

Atmospheric Chemistry and Dynamics Branch, NASA Goddard Space Flight Center, Greenbelt, Maryland

J. ERIC NIELSEN

Global Modeling and Assimilation Office, NASA Goddard Space Flight Center, Greenbelt, Maryland

(Manuscript received 30 November 2007, in final form 10 March 2008)

ABSTRACT

Past and future climate simulations from the Goddard Earth Observing System Chemistry–Climate Model (GEOS CCM), with specified boundary conditions for sea surface temperature, sea ice, and trace gas emissions, have been analyzed to assess trends and possible causes of changes in stratospheric water vapor. The simulated distribution of stratospheric water vapor in the 1990s compares well with observations. Changes in the cold point temperatures near the tropical tropopause can explain differences in entry stratospheric water vapor. The average saturation mixing ratio of a 20° latitude by 15° longitude region surrounding the minimum tropical saturation mixing ratio is shown to be a useful diagnostic for entry stratospheric water vapor and does an excellent job reconstructing the annual average entry stratospheric water vapor over the period 1950–2100. The simulated stratospheric water vapor increases over the 50 yr between 1950 and 2000, primarily because of changes in methane concentrations, offset by a slight decrease in tropical cold point temperatures. Stratospheric water vapor is predicted to continue to increase over the twenty-first century, with increasing methane concentrations causing the majority of the trend to midcentury. Small increases in cold point temperature cause increases in the entry water vapor throughout the twenty-first century. The increasing trend in future water vapor is tempered by a decreasing contribution of methane oxidation owing to cooling stratospheric temperatures and by increased tropical upwelling, leading to a near-zero trend for the last 30 yr of the twenty-first century.

1. Introduction

Water vapor is an important component of the chemistry and radiative balance (Forster and Shine 1999) of the stratosphere, and understanding and realistically modeling its distribution and trends are necessary for tackling many outstanding scientific questions, including the recovery of the ozone layer. Temperatures near the tropical tropopause control the entry values of water vapor into the stratosphere by limiting dehydrating air masses to their saturation mixing ratio as they ascend through this region (Brewer 1949). Combined with methane oxidation, this controls the water vapor budget of the stratosphere (Le Texier et al. 1988). General circulation models (GCMs) and chemistry–climate models (CCMs) can be very useful tools for understanding past and potential future changes to water vapor in the stratosphere. However, many models have difficulty accurately simulating temperatures in the

Corresponding author address: Luke Oman, Department of Earth and Planetary Sciences, The Johns Hopkins University, 301 Olin Building, 3400 North Charles Street, Baltimore, MD 21218.
E-mail: oman@jhu.edu

DOI: 10.1175/2008JAS2696.1

© 2008 American Meteorological Society

tropical tropopause region (e.g., Pawson et al. 2000; Eyring et al. 2006) and are therefore unable to properly simulate the mean state of stratospheric water vapor.

Holton and Gettelman (2001) proposed the cold trap hypothesis, suggesting that most of the air entering the stratosphere has been processed (dehydrated) by the coldest regions longitudinally within the tropics. Fueglistaler and Haynes (2005) similarly showed that stratospheric entry water vapor can be determined from the minimum saturation mixing ratio that the air mass goes through during ascent (the Lagrangian cold point). A number of studies examining the trend in water vapor over the past few decades have found varying results, from large increases using balloon measurements over Boulder, Colorado (Oltmans et al. 2000; Rosenlof 2002), to relatively small changes measured using the Halogen Occultation Experiment (HALOE) satellite (Randel et al. 2004). Although recent analysis (Scherer et al. 2007) has somewhat narrowed the gap, differences between these two dataset still remain. Randel et al. (2006) showed that there have been significant decreases in stratospheric water vapor since 2001, which are coincident with increased tropical upwelling and decreased tropical lower stratosphere ozone. These issues point to the need of fully coupled chemistry–climate models to properly simulate the feedbacks involved. Garcia et al. (2007) used the Whole Atmosphere Community Climate Model, version 3 (WACCM3) chemistry–climate model to simulate past trends in stratospheric water vapor and found it difficult to simulate the trends observed because of high interannual variability.

The earth's atmosphere is such a highly coupled system that the use of CCMs is required to best simulate past and future changes to stratospheric water vapor. Several recent studies have examined stratospheric moisture in CCMs (Austin et al. 2007; Garcia et al. 2007). In this paper we will analyze the trends and evolution of stratospheric water vapor in the Goddard Earth Observation System (GEOS) CCM (GEOS CCM). Section 2 contains a brief description of the model and the experiments used in this study. Section 3 analyzes the results of these model simulations and discusses causes of the trends produced. Finally, section 4 contains discussion and conclusions from this study.

2. Model

The GEOS CCM is described in Pawson et al. (2008). It is based on the GEOS Data Assimilation System, version 4 (GEOS-4) GCM (Bloom et al. 2005). In this study, the model was run at a resolution of 2° latitude by 2.5° longitude with 55 layers up to 80 km. The gas-phase stratospheric chemistry used in the model runs is from Douglass and Kawa (1999), with the representation of polar stratospheric clouds and their heterogeneous chemical impacts taken from Considine et al. (2003), as described in Stolarski et al. (2006).

The physical and chemical processes constraining water vapor are of great importance to this study. In the troposphere, moist processes are computed using the physical parameterizations from Kiehl et al. (1998), in which water vapor is predicted but a diagnostic cloud scheme is used, meaning that liquid water and ice are not retained between model time steps. Precipitating moisture from clouds may re-evaporate into the environment or reach the ground as rainfall. Condensation is prescribed to begin once the ambient humidity reaches 80% of the saturation value, and all excess moisture is assumed to condense once an air mass reaches its saturation specific humidity. This means that vapor is removed at the cold point temperature (CPT) when temperature reaches the saturation point, so the model does not allow supersaturated air (in excess of 100% RH) to pass into the stratosphere. Figure 1 illustrates this by showing a scatterplot of 100-hPa temperature (K) and specific humidity (ppmv), with filled circles indicating relative humidity above 99% for 1 January 2001. The geographic locations of these points are plotted over the temperature (K) between 30°S and 30°N to show the preferential regions for dehydration, which for January is over the Indo-Pacific (IP) region. In the stratosphere, the moisture field is under chemical control. The main factor impacting stratospheric moisture is the additional source caused by oxidation of methane (see Le Texier et al. 1988), which is represented in the chemistry code. In some regions, such as the cold Antarctic lower stratosphere, ice clouds form, resulting in dehydration of the air masses.

Two model simulations were used in this study. The first was run from 1950 to 2004 (past) using the Hadley SST and sea ice dataset from Rayner et al. (2003), which is derived from observations. The second (future) run, for 2000–99, was conducted with SST and sea ice data from an AR-4 integration of the National Center for Atmospheric Research (NCAR) Community Climate System Model, version 3 (CCSM3) atmospheric model. This model run followed the scenario A1b for greenhouse gas emissions from Houghton et al. (2001). The model simulations do not include the Quasi-Biennial Oscillation (QBO), condensed ice, or volcanic eruptions, which can impact tropical tropopause temperatures.

Most of the model analysis uses monthly mean fields; however, temperature data come from model restart files, representing an instantaneous snapshot of the first

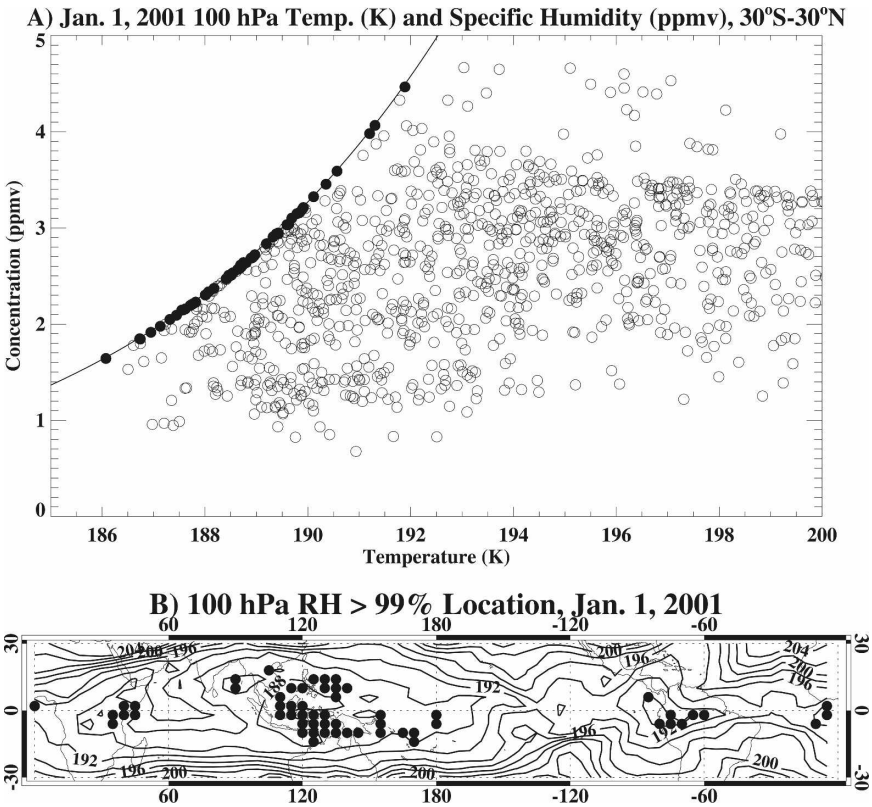

FIG. 1. (a) Scatterplot showing 100-hPa temperature (K) and specific humidity (ppmv) with filled circles indicating relative humidity above 99% for 1 Jan 2001. Also shown is the 100% relative humidity curve (solid line). (b) The geographic location of these points plotted over the temperature (K) between 30°S and 30°N.

day of each month, because the monthly average 85-hPa layer was not archived during these runs. A 10-yr subset was rerun, saving data at all these layers to confirm that once-monthly snapshots can reasonably well represent the variations in average monthly values over the tropical tropopause layer.

3. Results

a. Comparisons with observations

Before examining long-term changes in the simulated water vapor we first compare it with observed distribution in the 1990s. The annual average 1992–2002 zonal-mean specific humidity from GEOS CCM is shown as Fig. 2a and compares well with measurements taken from HALOE for the same period (Fig. 2b) (Grooß and Russell 2005). The average model concentrations vary from 3 ppmv in the tropical lower stratosphere to over 5.6 ppmv in the upper stratosphere in the extratropics and near the stratopause in the tropics. The spatial distribution agrees well with the observations, but the model has a low bias of about 0.4 ppmv throughout the stratosphere. This is due to a small cold bias at the cold point tropopause in the model, which results in a lower value of water vapor entering the stratosphere [see Fig. 7 of Eyring et al. (2006) for comparisons of GEOS CCM 100-hPa temperatures and water vapor with observations]. The tropical water vapor "tape recorder" in GEOS CCM also agrees well with observations, with good agreement in both the propagation speed and attenuation of amplitude [see Fig. 9 of Eyring et al. (2006)]. More detailed comparisons of GEOS CCM and other CCMs with HALOE are shown in Eyring et al. (2006), with GEOS CCM having one of the better simulated stratospheric water vapor concentrations. Also, comparisons with various CCMs and reanalysis data are shown in Gettelman et al. (2008). The model also has stronger subtropical mixing barriers and a slight tilt of the tropical pipe toward the Southern Hemisphere.

The linear trends over the same period from GEOS CCM and HALOE are compared in Figs. 2c and 2d. Generally we see negative trends in the lower stratosphere mostly over the tropics, with little if any trend in the mid and upper stratosphere. In the lower stratosphere the trend in HALOE (Fig. 2d) is also negative,

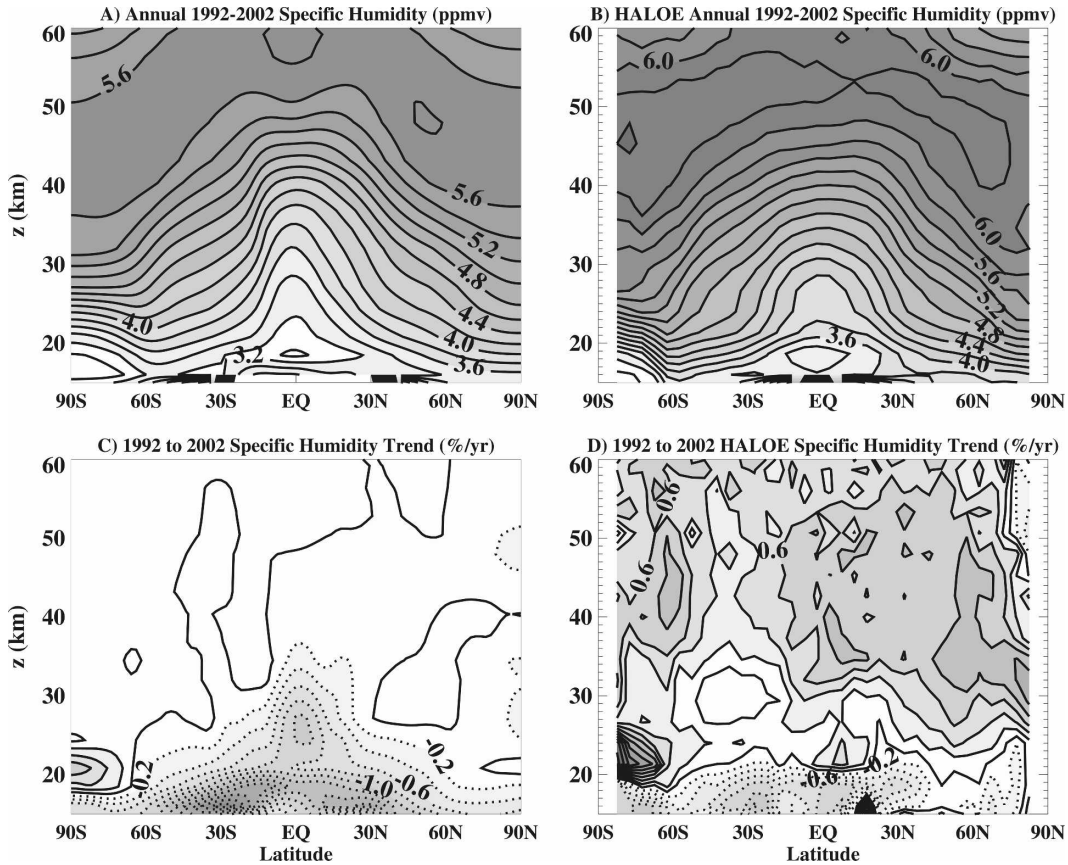

FIG. 2. (a), (b) Zonal mean annual average specific humidity (ppmv) from 15–60 km for (a) the model and (b) HALOE. (c), (d) The trend (in % yr^{-1}) over the years 1992–2002 for (c) the model and (d) HALOE.

but HALOE has a much larger positive trend in the mid to upper stratosphere. As discussed in Garcia et al. (2007), it is difficult to compare decadal-scale trends in climate models and observations because of the large variability in simulated decadal trends (i.e., very different trends are found for different decades in the simulation). Also, the QBO has an important impact on tropical tropopause temperature, which is not included in the model but could have an influence in the observational trends when examining shorter periods of time (e.g., 10 yr or less). In addition, there are different trends among HALOE and National Oceanic and Atmospheric Administration (NOAA) frostpoint observational datasets (Scherer et al. 2007).

b. *Stratospheric entry values*

The distribution of stratospheric water vapor is controlled by the values entering the stratosphere and methane oxidation within the stratosphere. We first examine variations in the "entry-value water vapor" (EWV). Figure 3 (black curves) shows the temporal variations of the annual average zonal mean stratospheric specific humidity at 70 hPa averaged between 10°S and 10°N, for both the past and future simulations. This acts as a proxy for the stratospheric water vapor entering the stratosphere. Although the tropical tropopause is typically near 100–85 hPa, it is the cold point temperature that determines the aridity of the stratosphere, which is above the tropical tropopause. The next standard pressure level is 70 hPa and because methane oxidation is insignificant at this level, the water vapor concentration can be taken as the entry value. This figure shows that there was a slight decrease in the EWV for the simulation of the past 50 yr, but a slight increase in the simulation over the next 100 yr.

To understand what controls the variations in EWV, we examine the temperature at the tropical tropopause. Figure 3a shows the annual average tropical (10°S–10°N) temperature for the three model layers around the tropical tropopause (100, 85, and 70 hPa) for the past (left) and future (right) runs. Figure 3a shows that there is cooling at 70 hPa but near-constant temperatures or warming at 85 and 100 hPa. Comparisons of these temperature changes with the 70-hPa specific

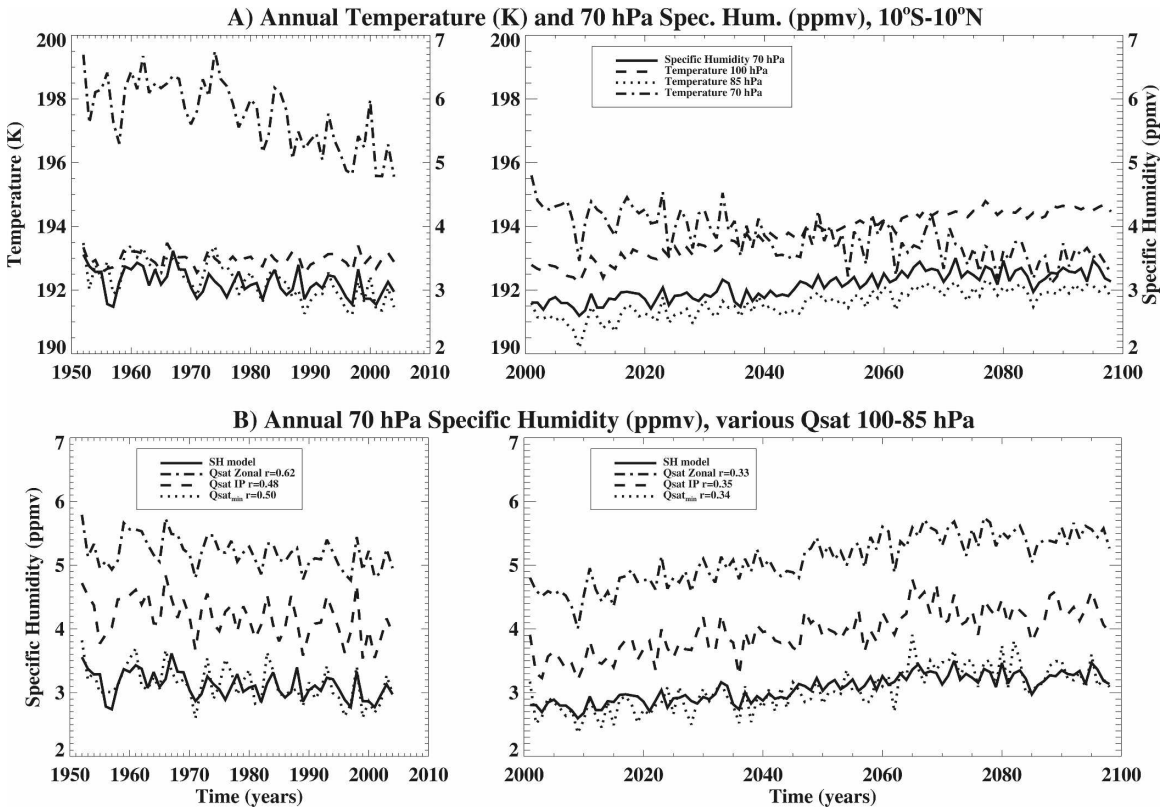

FIG. 3. (a) Annual average zonal mean (10°S–10°N) temperatures (K) at 100 (dashed line), 85 (dotted line), and 70 hPa (dashed–dotted line) for the (left) past and (right) future simulations. Also shown is the annual average zonal mean stratospheric specific humidity (ppmv) at 70 hPa from 10°S to 10°N representing the stratospheric water vapor at entry (solid line). (b) Annual average zonal mean tropical (10°S–10°N) stratospheric water vapor (ppmv) at entry (70 hPa; solid line) compared to various saturation mixing ratio (Qsat) measurements using 100- or 85-hPa temperatures for the zonal mean (10°S–10°N; dashed–dotted line), the IP region (10°S–10°N, 80°–180°E; dashed line), and $Qsat_{min}$ (dotted line), which is a 20° latitude by 15° longitude average surrounding the minimum value for the (left) past and (right) future simulations. Also shown are the detrended Pearson correlation coefficients of each with the modeled tropical stratospheric water vapor at entry.

humidity (10°S–10°N), show that the water vapor changes are very similar to those in the 85-hPa temperature.

To examine the relationship between EWV and tropopause temperatures more quantitatively, we examine the minimum saturation mixing ratio ($Qsat_{min}$), which is a function of both temperature and pressure. In GEOS CCM $Qsat_{min}$ and CPT are typically at 85 hPa, but this varies somewhat depending on season and between the past and future runs. During the boreal winter, when the tropopause is seasonally highest, the CPT and $Qsat_{min}$ are at 85 hPa nearly all of the time, whereas during boreal summer, when the tropopause is lowest, there is a transition over time. In the past run the summer CPT and $Qsat_{min}$ occurs more often at 100 hPa, whereas in the future run they are more often at 85 hPa. This transition occurs in the first part of the twenty-first century. It is not until the last 15 yr of the past simulation that the 85-hPa temperatures are about 1 K colder then the 100-hPa temperatures, showing the transition of $Qsat_{min}$ on an annual basis.

The EWV is compared to various measures of Qsat over the tropical tropopause layer in Fig. 3b. First consider the tropical (10°S–10°N) average Qsat (dashed–dotted line). This time series was calculated by selecting the minimum value of monthly mean Qsat between the 100- and 85-hPa layers, and then annually averaging. The temporal variations in this zonal mean Qsat and EWV are very similar (with a correlation coefficient r of 0.62 and 0.33 for the past and future runs, respectively). However, the zonal mean Qsat is larger by around 2 ppmv. This offset is likely because of large longitudinal variability in tropical tropopause temperatures and the fact that air masses are more likely to be processed (dehydrated) by the coldest regions within this zonal band (Holton and Gettelman 2001). We therefore consider (dashed line) Qsat averaged over the IP region (10°S–10°N, 80°–180°E), which corre-

sponds to a warm pool of sea surface temperatures and an area of enhanced convection. In the tropical tropopause layer, this area is generally colder than the zonal mean average, especially during boreal winter when convective activity is seasonally largest. Over the course of the past and future runs, the IP Qsat is typically about 1–1.5 ppmv less than the zonal mean Qsat, and in better agreement with EWV. However, there is still a bias between the IP Qsat and EWV, and we therefore consider a third region. The dotted line represents the $Qsat_{min}$ calculated by looking for the minimum temperature between 30°S and 30°N and averaging the neighboring grid box cells (±10° latitude and ±7.5° longitude). This value does an excellent job reproducing both the temporal variability (r = 0.5 and 0.34 for past and future runs) and magnitude of the stratospheric entry specific humidity over both the past and future runs (Fig. 3b, left and right, respectively). Therefore, in GEOS CCM, changes in $Qsat_{min}$ for the coldest region of the tropical tropopause can be used to explain or diagnose changes in the water vapor entering the stratosphere.

LOCATIONS OF $QSAT_{MIN}$

It is important to note that the location of the $Qsat_{min}$ will vary depending on the time of year, so a fixed area cannot faithfully represent what controls the absolute magnitude of stratospheric water vapor at entry. We can examine the model's location for $Qsat_{min}$ during our past runs to see how this location changes depending on the time of year. Dividing the year into two time periods separates the dominant locations of $Qsat_{min}$. Figure 4a shows the months of November–April, in which the majority of events occur in the area over the western Pacific Warm Pool. It can be seen both here and in Fig. 1b that the coldest temperatures and a good deal of the dehydration occur over the western Pacific Warm Pool. This is in contrast to the months of May through October (Fig. 4b) in which the Indian monsoon region dominates, with a secondary maximum over Central America. It is these areas (shown in Figs. 4a,b) that are critical in determining the absolute dryness of the stratosphere in our model simulations.

c. *Methane oxidation*

Changes in the stratospheric water vapor occur not only because of changes in EWV but also because of changes in methane oxidation. To understand the role of methane oxidation, we use the approximation (Austin et al. 2007)

$$H_2O(\theta, p, t) = H_2O|_e(t - \tau) + 2[CH_4|_0(t - \tau) - CH_4(\theta, p, t)], \quad (1)$$

where $H_2O|_e$ is tropical specific humidity at 70 hPa, $CH_4|_0$ is tropical methane at 150 hPa, and τ is the mean age of air. The first term on the right-hand side is the entry water vapor; the second is production by methane oxidation. By examining the trends in stratospheric water vapor caused by each term, we can see the relative importance of each in the overall trend.

We first consider how well (1) can reproduce the simulated water vapor. Figure 5a shows the simulated stratospheric water vapor for 1992–2002, which is the same quantity shown in Fig. 1a. The second half of Eq. (1), which indicates water vapor resulting from methane oxidation, is shown as Fig. 5b. Methane oxidation is near zero at the tropical tropopause and rises to over 2 ppmv in upper stratosphere. The percentage of water vapor in the stratosphere resulting from methane oxidation is typically less than 50% except in the extratropical upper stratosphere, where the two components (EWV and methane oxidation) are approximately equal. Figure 5c shows the methane oxidation concentrations added to the EWV, which is from the first half of Eq. (1). The difference between this constructed water vapor and the simulated water vapor is shown in Fig. 5d. For the bulk of the stratosphere the differences are very close to zero; only where there are water vapor sinks are there significant differences. In the Southern Hemisphere the model is drier over Antarctica from 15–30 km because of local dehydration in the polar vortex from polar stratospheric cloud formation. There is also loss in the mesosphere because of its reaction with $O(^1D)$ and solar Lyman α photolysis, in which H_2 is formed by the destruction of water vapor (Brasseur and Solomon 1986).

We now consider changes in water vapor over the past simulation. Figure 6a shows the simulated changes in zonal mean water vapor from 1956–65 to 1995–2004. Over this period there is a decrease in the lower stratosphere, especially in the tropics, and an increase throughout the remainder of the stratosphere, peaking at 0.6 ppmv in the extratropical stratopause. The methane oxidation term [second term on the right-hand side of Eq. (1)] over that same time period is shown in Fig. 6b; it is positive everywhere and increases from near zero at the tropical lower stratosphere to 0.9 ppmv in the extratropical stratopause. This is caused by an increase in tropospheric methane. Over this time period, the tropical tropopause cools by an amount equal to a change of around −0.25 ppmv in stratospheric entry specific humidity (see Fig. 3), calculated from a linear trend. Figure 6c shows the reconstructed stratospheric water vapor using Eq. (1) (i.e., the change in water vapor at 70 hPa plus the methane oxidation shown in Fig. 6b). This reconstructed change in water vapor com-

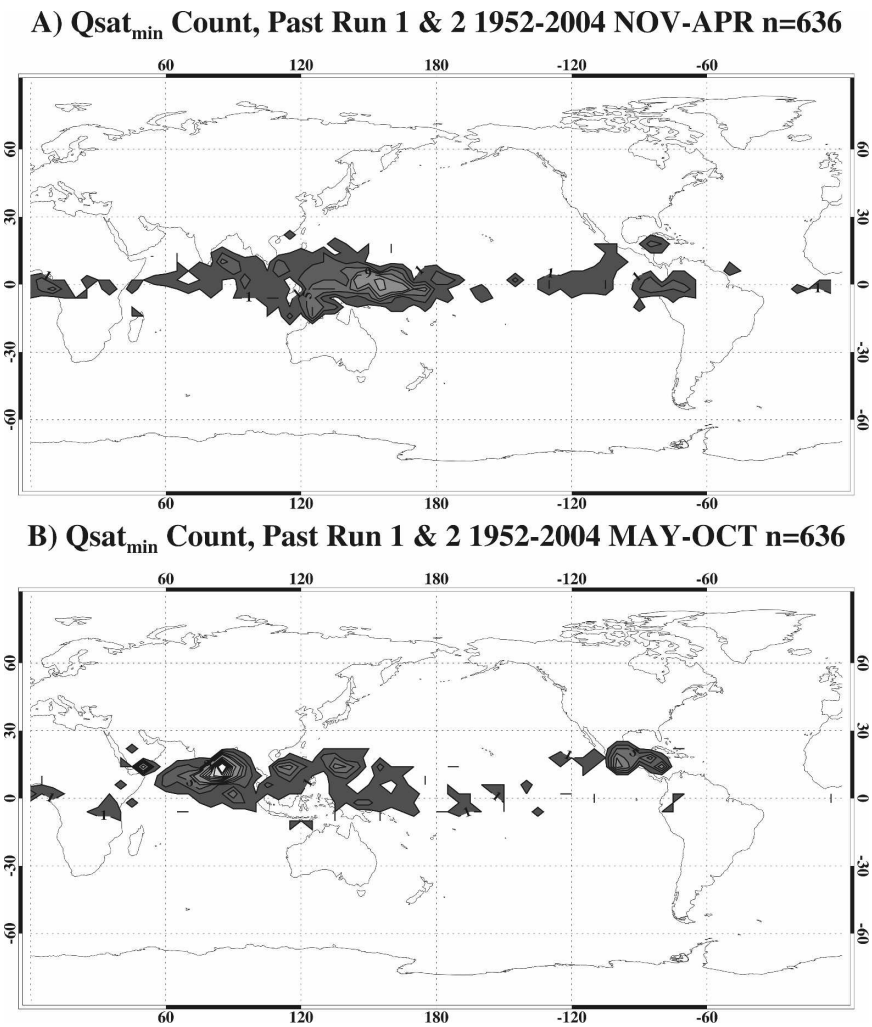

FIG. 4. Count of the Qsat$_{min}$ locations for past runs 1 and 2 for (a) November–April and (b) May–October for 1952–2004.

pares well to the model changes in water vapor, especially in the Northern Hemisphere. In the Southern Hemisphere, the model is drier over Antarctica from 15 to 30 km because of more local dehydration in the polar vortex. There are also small positive anomalies in the extratropical upper stratosphere and stratopause that indicate that the model is slightly drier than the constructed values. This drier air is likely due to downwelling of mesospheric air. Comparison of Figs. 6a and 6b shows that methane oxidation is the main cause of the increase in modeled water vapor in the middle and upper stratosphere from 1956–65 to 1995–2004.

Similar calculations for the future simulation show a very different picture. The simulated changes in specific humidity from 2006–15 to 2089–98 (Fig. 7a) have a different spatial variation than the changes from 1956–65 to 1995–2004 (Fig. 6a). For the future period there is an increase in the tropical lower stratosphere, a decrease in the Antarctic lower stratosphere, and a more uniform increase throughout the middle and upper stratosphere. These differences in the structure of the past and future trends are largely because of differences in methane oxidation. Methane monotonically increases in the past simulation, but in the future simulation tropospheric concentrations peak around 2050 and then begin to decrease. As a result, the methane oxidation contribution to the future water vapor trend is much smaller than in the past, and there is even a small negative contribution in the lower stratosphere (cf. Figs. 7b and 6b). The change in tropical tropopause temperatures over this time corresponds to 0.5 ppmv increase in entry specific humidity (see Fig. 3), calculated from a linear trend. Figure 7c shows the constructed change in water vapor on average is 0.5 ppmv, which is mostly due

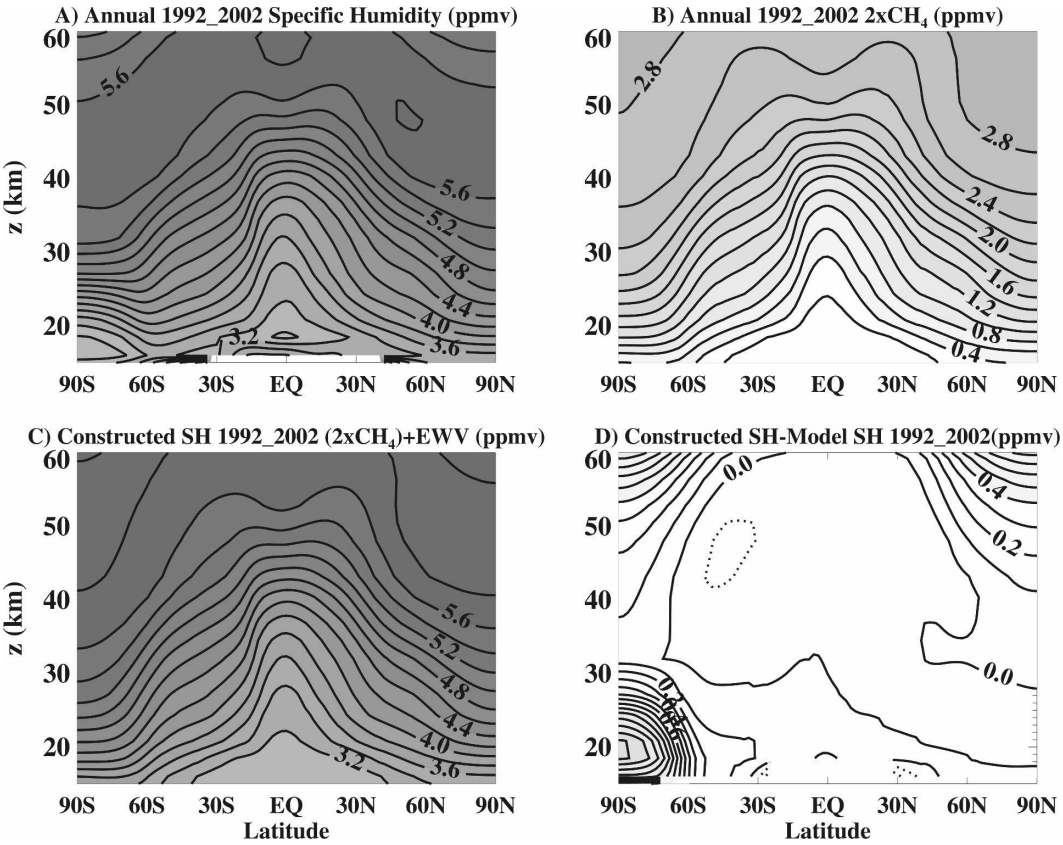

FIG. 5. (a) Model stratospheric water vapor (ppmv) from 1992 to 2002. (b) Stratospheric water vapor produced by 2 × methane oxidation (ppmv) during the same time period. (c) As in Fig. 5b, but plus the EWV over that time period. (d) The difference between (c) constructed and (a) model water vapor.

to the change in EWV, with the largest trend over the mid and upper extratropical stratosphere where there is a greater contribution from methane oxidation. The differences in model and constructed specific humidity are shown in Fig. 7d and are generally small except for the change due to Antarctic polar dehydration. There is about 0.25 ppmv less water vapor in the Antarctic polar lower stratosphere by the end of the twenty-first century. This is due to an approximate −2 K temperature change during June–August over this time period, resulting in 1 ppmv less water vapor (dividing by 4 gives the annual response). This suggests increases in polar stratospheric cloud formation during these months. If we were to consider just the first half of the twenty-first century, then the trend would be dominated by changes in tropospheric methane concentrations, with an additional impact from a small warming of the CPT.

Comparison of Figs. 6 and 7 shows that the relative contributions of methane oxidation to trends in water vapor are dependent on the time period considered. Methane oxidation is the largest contribution to the trends in middle and upper stratospheric water vapor in the past 50 yr, but this is not the case for the trend over the twenty-first century. Only when considering the first half of the twenty-first century is methane oxidation still the dominant factor. To illustrate the changes in relative contributions to trend, Fig. 8 shows the annual time series of simulated water vapor (solid line), reconstructed specific humidity (dotted line) and contributions from EWV (dashed–dotted line) and methane oxidation (dashed line) for two locations at 3 hPa. From this it can be seen that although EWV has a slow and steady increase over the future simulation, the contribution of methane oxidation to the trend peaks around 2050 and decreases after that, so by the end of the twenty-first century methane oxidation returns to values typical of the beginning of the century. This causes changes in the entry water vapor to be the main contribution to the water vapor trend over the entire century. Figure 8b shows the time series at 86°S and 3 hPa and in general agrees well, although there are some small differences. As mentioned before, the model has a small dry bias versus the reconstructed time series due to the impact of downwelling mesospheric air. This is

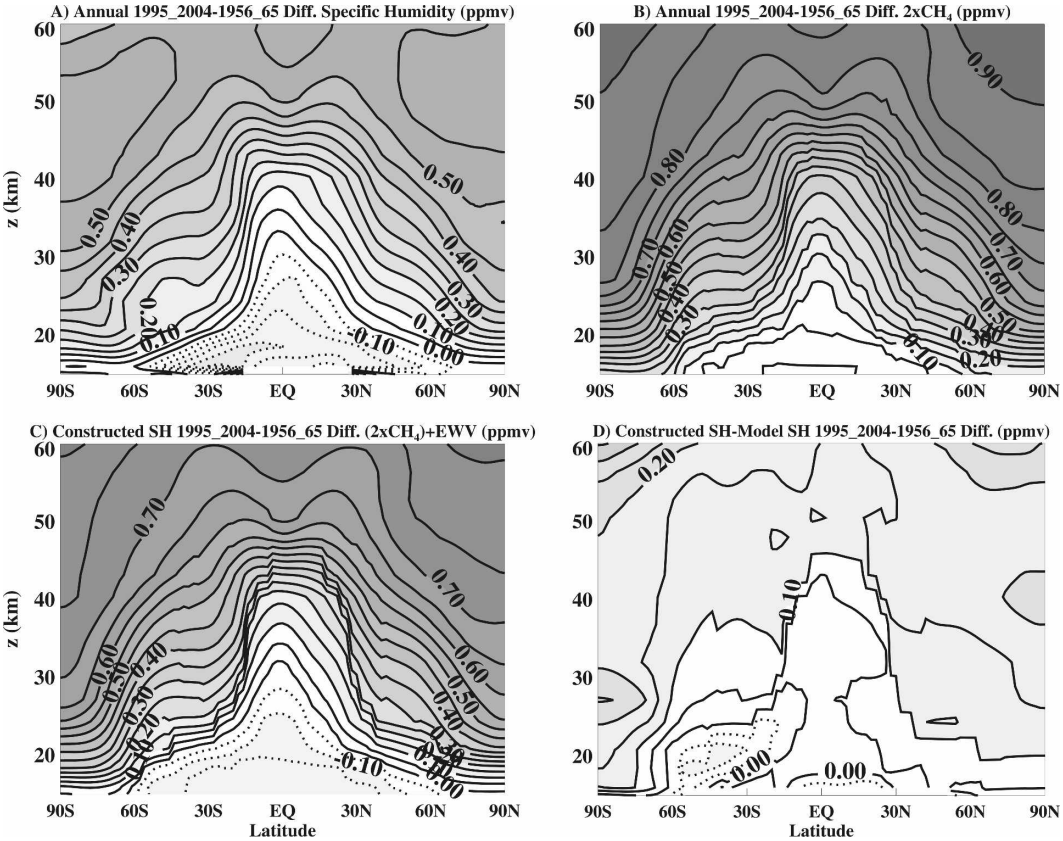

FIG. 6. As in Fig. 5, but for 1956–65 to 1995–2004.

not present over the equator in Fig. 8a where there is generally upwelling, and the magnitude of this difference is larger over the south polar region compared to the north polar region (not shown) because downwelling there is larger above 10 hPa.

Although changes in the tropospheric concentration of methane are the primary cause of changes in the production of water vapor by methane oxidation, it is also possible that changes in stratospheric temperatures and circulation could cause changes in the amount of methane oxidation. Over the period of the future simulation there is a significant cooling in upper stratosphere (~ -7K at 3 hPa) from increasing CO_2, which results in a decrease in the methane oxidation rate. Using the modified Arrhenius expression (Brasseur et al. 1999), the reaction rate between OH and methane decreases about 14% for a 5 K decrease in temperature (over typical stratospheric temperature values). A 5 K decrease is an average mid to upper stratospheric temperature change over this time period. This change in oxidation rate can explain most of the approximate 15% decrease in methane oxidation seen in our simulations. There is also an increase in tropical upwelling (decrease in mean age), which also results in a reduction in methane oxidation; however, this impact is much smaller than that caused by temperature.

To examine the impact of these changes, we compare in Fig. 9 the model methane loss at two upper stratospheric locations, calculated as in Eq. (1) (solid curve) with that which would have been produced assuming fixed circulation and temperatures in the future (dashed). The later quantity was calculated by first calculating the annual average percentage methane loss (methane lost at a location as a percentage of that entering the stratosphere) for 2006–15 and then applying this to the complete tropospheric methane time series. Figure 9 shows that in the model less methane is oxidized than in the case of fixed temperature and circulation. By the end of the century, the difference at the equator is about 0.1 ppmv (which equates to about 0.2 ppmv less water vapor), whereas at 86°S the difference is about 0.15 ppmv (0.3 ppmv less water vapor). The main cause of this reduced methane oxidation is decreasing stratospheric temperatures (reducing oxidation rates) with additional contributions from increasing stratospheric circulation. This change in methane oxidation over time is especially significant considering that the model change in water vapor over the twenty-

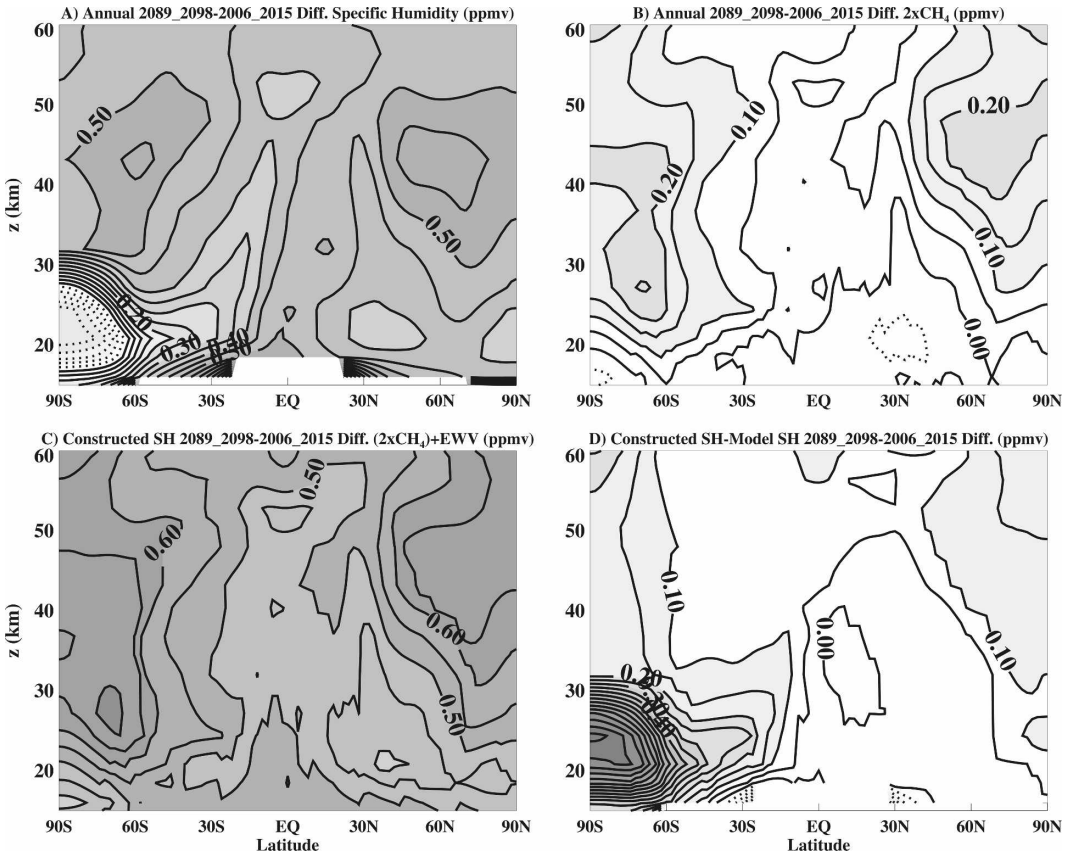

FIG. 7. As in Fig. 5, but for 2006–15 to 2089–98.

first century is about 0.5–0.6 ppmv. Without this offsetting factor associated with temperature and transport changes, the upper stratospheric water vapor changes would have been about 30%–40% larger.

d. Controls on cold point temperatures

To fully understand any trends in the simulated stratospheric water vapor, the factors controlling the CPT are examined. The tropopause temperature response represents a balance of changes in the upper troposphere and lower stratosphere. Tropical upper tropospheric temperatures are mainly controlled by moist convective adjustment from changes in tropical SSTs. An increase in SSTs from rising greenhouse gas concentrations corresponds to increased upper tropospheric temperatures. There is no direct correlation between tropical SSTs and 85-hPa temperatures ($r = -0.01$) in the model simulations. In the lower stratosphere, ozone and upwelling changes have the largest impact on temperatures. Decreasing ozone and increased upwelling, which have been noticed in recent years (Randel et al. 2006), both have cooling impacts on the lower stratosphere. There are additional factors that are important at the tropical tropopause in the real atmosphere that are not included in these simulations, like the QBO and condensed ice.

To estimate the relative role of changes in SSTs, lower stratospheric ozone, and lower stratospheric upwelling in causing the changes in tropical tropopause temperatures, we perform a multiple linear regression analysis. Figure 10a compares the annual average 20°S–20°N 85-hPa temperatures (K; solid line) with a reconstructed time series using multiple linear regression of three variables from the model runs: tropical (20°S–20°N) SSTs, 70-hPa ozone, and 70-hPa w^* (dotted line) for the future run. The tropical 85-hPa temperature and reconstructed time series are highly correlated ($r = 0.77$), with similar results over the past run (not shown). Figure 10b shows the relative contribution of the three variables to the regression analysis. The black line shows the contribution from tropical SSTs for the twenty-first century, which is approximately a 4.5 K warming. This strong warming in the upper troposphere is somewhat balanced by cooling influences in the lower stratosphere. In the tropical lower stratosphere (70 hPa) we see a 20% decrease in ozone, which

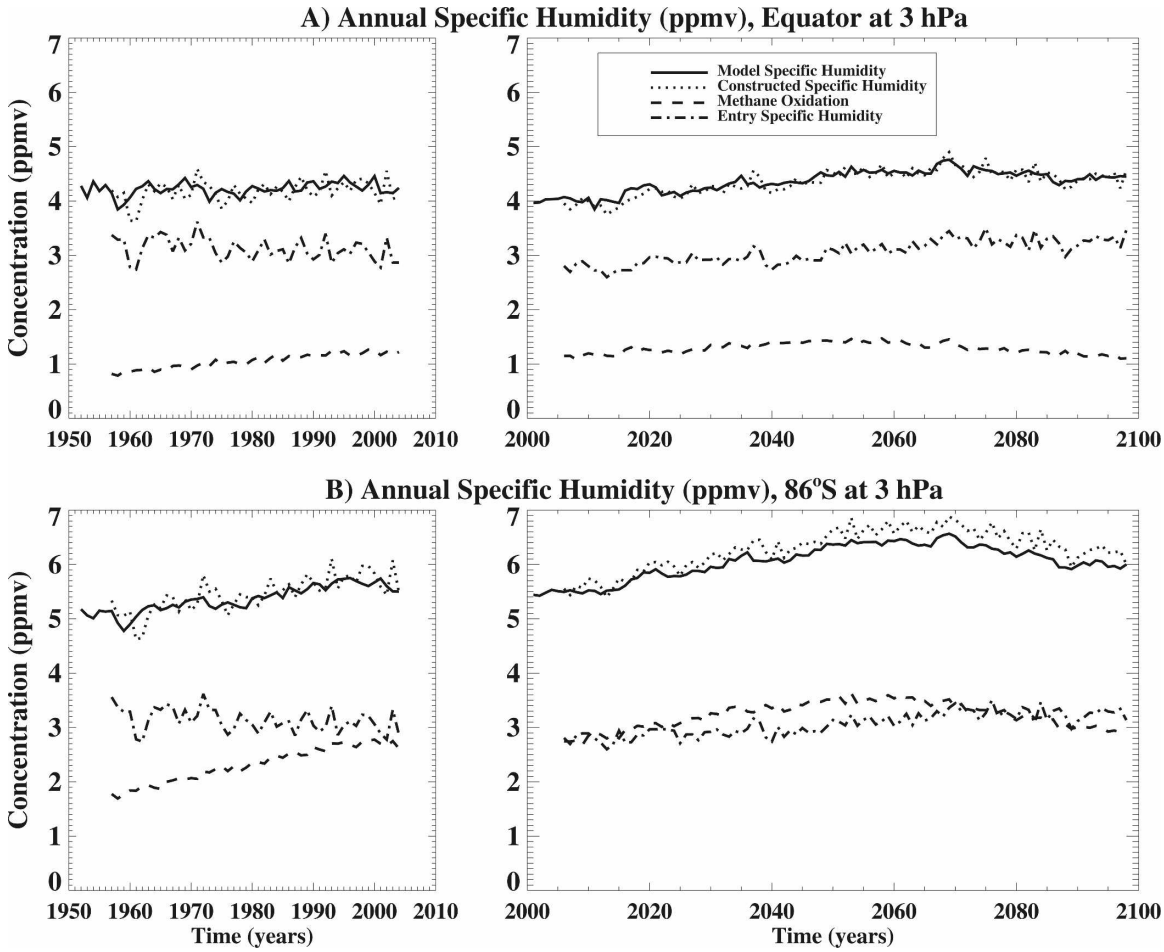

FIG. 8. Time series of model specific humidity (solid line) and constructed specific humidity (dotted line). Constructed specific humidity is formed by adding 2x methane oxidation (dashed line) to entry specific humidity (dashed–dotted line). All values are in ppmv.

results from increased upwelling, contributing to a 2 K decrease in temperature. Changes in tropical upwelling can also directly impact temperatures, with increased upwelling causing adiabatic cooling. Over the twenty-first century, in our simulations we see a 30% increase in tropical upwelling (using w^* as a proxy), corresponding to an approximately −1.2 K change in temperature.

There are, however, significant correlations among

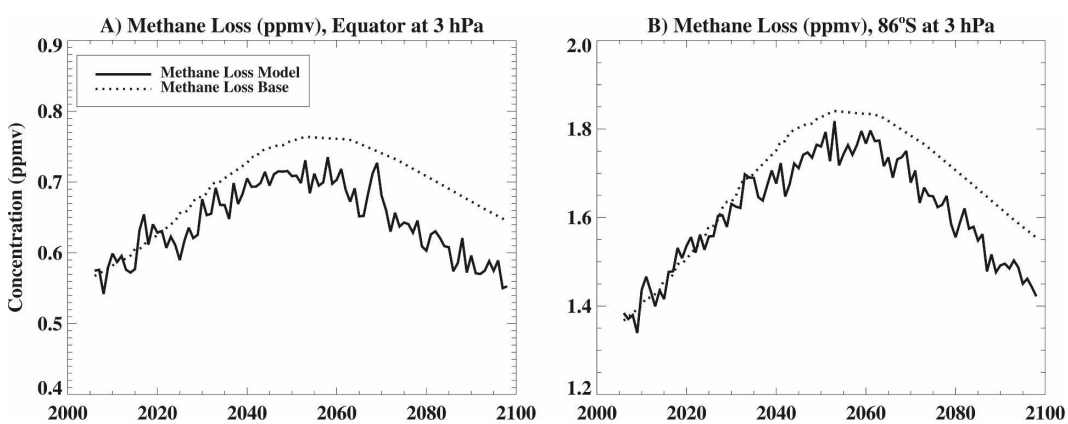

FIG. 9. Methane loss calculated from the model compared to a base case assuming no changes to temperature and circulation for a point (a) over the equator at 3 hPa and (b) over 86°S at 3 hPa over the future run.

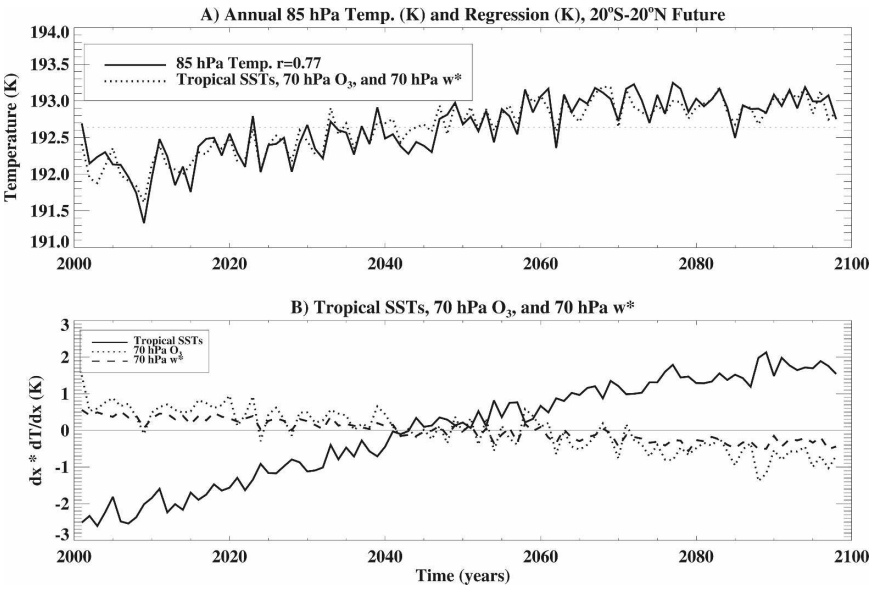

FIG. 10. (a) Annual mean 20°S–20°N 85-hPa temperature (K; solid line) and a multiple linear regression (dotted line) created from tropical (20°S–20°N) SSTs, 70-hPa O_3, and 70-hPa w^* for the future run. The detrended Pearson correlation is 0.77. (b) Relative contribution of tropical (20°S–20°N) SSTs (solid line), 70-hPa O_3 (dotted line), and 70-hPa w^* (dashed line) in the regression analysis.

these three variables, so it is important to determine if the regression analysis can correctly separate the relative contributions to CPT. We do this by comparing the sensitivities from the multiple linear regression analysis with other estimates.

Linear trend analysis of the 150-hPa temperature in the future model simulation shows approximately 4.5 K warming over the twenty-first century, which agrees well with the increase due to warming tropical SSTs in the regression analysis. The sensitivity to changes in ozone can be compared with the results of Forster et al. (2007). They used a fixed dynamical heating model to simulate the change in temperature in the lower stratosphere from the recent observed decrease in ozone and found approximately a 0.6 K decrease in temperature at 70 hPa from a 6% change in ozone. This agrees well with a −2 K change for 20% ozone reduction, assuming a linear relationship over these values. The sensitivity to changes in upwelling is compared with analysis of a previous model experiment with fixed ozone. In this previous simulation a 10% increase in tropical upwelling corresponded to a −0.5 K decrease in temperature at 70 hPa. Again, assuming a linear relation over our values yields a 1.5 K decrease in temperature for a 30% increase in tropical upwelling, in good agreement with our −1.2 K. The above comparisons indicate that the multiple linear regression analysis is able to reasonably separate the relative contributions to the CPT. It is important to note that the radiative cooling influence of ozone decreases on the CPT and that models that use fixed ozone or ozone that does not respond to changing stratospheric circulation could overestimate future trends in CPT and thus stratospheric water vapor.

4. Conclusions

We have analyzed trends and possible causes of changes in stratospheric water vapor in past and future climate simulations from the GEOS CCM. This paper shows that the GEOS CCM can reasonably reproduce the observed mean state of stratospheric water vapor in the 1990s.

Changes in the entry stratospheric water vapor can be explained by changes in cold point temperatures (CPTs) near the tropical tropopause. It is shown both that the coldest area longitudinally within the tropics sets the magnitude of stratospheric water vapor at entry and that the average saturation mixing ratio over a 20° latitude by 15° longitude grid box centered about the minimum saturation mixing ratio ($Qsat_{min}$) can reproduce interannual variability and trends in entry stratospheric water vapor over 1950–2100. The CPT and $Qsat_{min}$ are somewhat seasonally dependent with the height of the tropopause. During boreal winter when the tropopause is highest, the CPT and $Qsat_{min}$ are nearly always at 85 hPa from 1950 to 2100 in our model simulations. During boreal summer when the tropo-

pause is lowest, $Qsat_{min}$ starts out at 100 hPa and transitions to 85 hPa near the beginning of the twenty-first century. The location of the $Qsat_{min}$ varies with the time of year, coinciding with areas of maximum convection. During November–April the main area is over the Western Pacific Warm Pool; during May–October this dominant region shifts toward the Indian monsoon region.

The simulated stratospheric water vapor trends were shown to be reproduced using changes in entry specific humidity and methane oxidation, except in the Antarctic polar vortex and mesosphere where there are water vapor sinks in the model. These reconstructions were then used to determine the relative role of changes in tropical tropopause temperatures (and hence entry value water vapor) and methane contributions.

The simulated stratospheric water vapor increases over the 50 yr between 1950 and 2000. There is only a slight decrease in tropical CPTs and hence entry water vapor, over this period, and the increase in water vapor is due primarily to increases in methane. In the future, stratospheric water vapor is predicted to continue to increase, with increasing methane concentrations causing the majority of the trend to midcentury. Surface methane concentrations peak around 2050 in the greenhouse gas scenario used in the future simulation, and small increases in cold point temperature cause increases in the entry water vapor throughout the twenty-first century. The increasing trend in future water vapor is tempered by a decreasing contribution of methane oxidation due to cooling stratospheric temperatures and increased tropical upwelling, leading to a near-zero trend for the last 30 yr of the twenty-first century.

There are only weak trends in entry water vapor in the simulations because CPTs are very stable from 1950 to 2100, remaining within 1 K over the whole period. At 100 hPa the warming trend is about twice as large (2 K) over this time, with even larger trends in the tropical upper troposphere. This is in contrast to the large cooling trend of about 6 K over this time at 70 hPa. The simulation suggests that the increased tropical upwelling has a negative impact on tropical tropopause temperatures, both directly through adiabatic cooling and indirectly through diabatic cooling as a radiative response to decreased ozone. Thus, the large positive temperature trends over the 150 yr of simulation in the upper troposphere are partially balanced by large negative trends in the lower stratosphere, causing a relatively small (<1 K) change in temperature at the CPT.

The methods used here for extracting stratospheric water vapor at entry and its trend should be tested with output from other models to evaluate its robustness. This could be a very helpful method for understanding future stratospheric water vapor trends.

Acknowledgments. We thank Paul Newman and Anne Douglass for their helpful comments and suggestions and Stacey Frith for helping with the data processing. Thanks to Stefan Fueglistaler and two anonymous reviewers for their helpful comments on improving this manuscript. We also appreciate Don Anderson of NASA's MAP Program for funding, those involved in model development at GSFC, and high-performance computing resources on NASA's "Project Columbia."

REFERENCES

Austin, J., J. Wilson, F. Li, and H. Vömel, 2007: Evolution of water vapor concentrations and stratospheric age of air in coupled chemistry–climate model simulations. *J. Atmos. Sci.,* **64,** 905–921.

Bloom, S., and Coauthors, 2005: The Goddard Earth Observation System Data Assimilation System, GEOS DAS version 4.0.3: Documentation and validation. NASA Tech. Memo. TM-2005-104606, Vol. 26, 166 pp.

Brasseur, G. P., and S. Solomon, 1986: *Aeronomy of the Middle Atmosphere*. 2nd ed. D. Reidel, 452 pp.

——, J. J. Orlando, and G. S. Tyndall, Eds., 1999: *Atmospheric Chemistry and Global Change.* Oxford University Press, 654 pp.

Brewer, A. W., 1949: Evidence for a world circulation provided by the measurements of helium and water vapour distribution in the stratosphere. *Quart. J. Roy. Meteor. Soc.,* **75,** 351–363.

Considine, D. B., S. R. Kawa, M. R. Schoeberl, and A. R. Douglass, 2003: N_2O and NO_y observations in the 1999/2000 Arctic polar vortex: Implications for transport processes in a CTM. *J. Geophys. Res.,* **108,** 4170, doi:10.1029/2002JD002525.

Douglass, A. R., and S. R. Kawa, 1999: Contrast between 1992 and 1997 high-latitude spring Halogen Occultation Experiment observations of lower stratospheric HCl. *J. Geophys. Res.,* **104,** 18 739–18 754.

Eyring, V., and Coauthors, 2006: Assessment of temperature, trace species, and ozone in chemistry–climate model simulations of the recent past. *J. Geophys. Res.,* **111,** D22308, doi:10.1029/2006JD007327.

Forster, P. M., and K. P. Shine, 1999: Stratospheric water vapour changes as a possible contributor to observed stratospheric cooling. *Geophys. Res. Lett.,* **26,** 3309–3312.

——, G. Bodeker, R. Schofield, S. Solomon, and D. Thompson, 2007: Effects of ozone cooling in the tropical lower stratosphere and upper troposphere. *Geophys. Res. Lett.,* **34,** L23813, doi:10.1029/2007GL031994.

Fueglistaler, S., and P. H. Haynes, 2005: Control of interannual and longer-term variability of stratospheric water vapor. *J. Geophys. Res.,* **110,** D24108, doi:10.1029/2005JD006019.

Garcia, R. R., D. R. Marsh, D. E. Kinnison, B. A. Boville, and F. Sassi, 2007: Simulation of secular trends in the middle atmosphere, 1950–2003. *J. Geophys. Res.,* **112,** D09301, doi:10.1029/2006JD007485.

Gettelman, A., and Coauthors, 2008: The tropical tropopause layer 1960–2100. *Atmos. Chem. Phys. Discuss.,* **8,** 1367–1413.

Grooß, J.-U., and J. M. Russell III, 2005: Technical note: A stratospheric climatology for O_3, H_2O, CH_4, NO_x, HCl, and HF

derived from HALOE measurements. *Atmos. Chem. Phys.,* **5,** 2797–2807.

Holton, J. R., and A. Gettelman, 2001: Horizontal transport and the dehydration of the stratosphere. *Geophys. Res. Lett.,* **28,** 2799–2802.

Houghton, J. T., Y. Ding, D. J. Griggs, M. Noguer, P. J. van der Linden, X. Dai, K. Maskell, and C. A. Johnson, Eds., 2001: *Climate Change 2001: The Scientific Basis*. Cambridge University Press, 881 pp.

Kiehl, J. T., J. J. Hack, G. B. Bonhan, B. A. Boville, D. L. Williamson, and P. J. Rasch, 1998: The National Center for Atmospheric Research Community Climate Model: CCM3. *J. Climate,* **11,** 1131–1149.

Le Texier, H., S. Solomon, and R. R. Garcia, 1988: The role of molecular hydrogen and methane oxidation in the water vapour budget of the stratosphere. *Quart. J. Roy. Meteor. Soc.,* **114,** 281–295.

Oltmans, S. J., H. Vömel, D. J. Hofmann, K. Rosenlof, and D. Kley, 2000: The increase in stratospheric water vapor from balloon borne frostpoint hygrometer measurements at Washington, D.C. and Boulder, Colorado. *Geophys. Res. Lett.,* **27,** 3453–3456.

Pawson, S., and Coauthors, 2000: The GCM–Reality Intercomparison Project for SPARC (GRIPS): Scientific issues and initial results. *Bull. Amer. Meteor. Soc.,* **81,** 781–796.

——, R. S. Stolarski, A. R. Douglass, P. A. Newman, J. E. Nielsen, S. M. Frith, and M. L. Gupta, 2008: Goddard Earth Observing System Chemistry–Climate Model simulations of stratospheric ozone-temperature coupling between 1950 and 2005. *J. Geophys. Res.,* **113,** D12103, doi:10.1029/2007JD009511.

Randel, W. J., F. Wu, S. J. Oltmans, K. Rosenlof, and G. E. Nedoluha, 2004: Interannual changes of stratospheric water vapor and correlations with tropical tropopause temperatures. *J. Atmos. Sci.,* **61,** 2133–2148.

——, ——, H. Vömel, G. E. Nedoluha, and P. Forster, 2006: Decreases in stratospheric water vapor after 2001: Links to changes in the tropical tropopause and the Brewer–Dobson circulation. *J. Geophys. Res.,* **111,** D12312, doi:10.1029/2005JD006744.

Rayner, N. A., D. E. Parker, E. B. Horton, C. K. Folland, L. V. Alexander, D. P. Rowell, E. C. Kent, and A. Kaplan, 2003: Global analyses of sea surface temperature, sea ice, and night marine air temperature since the late nineteenth century. *J. Geophys. Res.,* **108,** 4407, doi:10.1029/2002JD002670.

Rosenlof, K. H., 2002: Transport changes inferred from HALOE water and methane measurements. *J. Meteor. Soc. Japan,* **80,** 831–848.

Scherer, M., H. Vömel, S. Fueglistaler, S. J. Oltmans, and J. Staehelin, 2007: Trends and variability of midlatitude stratospheric water vapour deduced from the re-evaluated Boulder balloon series and HALOE. *Atmos. Chem. Phys. Discuss,* **7,** 14 511–14 542.

Stolarski, R. S., A. R. Douglass, M. Gupta, P. A. Newman, S. Pawson, M. R. Schoeberl, and J. E. Nielsen, 2006: An ozone increase in the Antarctic summer stratosphere: A dynamical response to the ozone hole. *Geophys. Res. Lett.,* **33,** L21805, doi:10.1029/2006GL026820.